

Thermodynamically consistent machine learning model for excess Gibbs energy

Marco Hoffmann^{1†}, Thomas Specht^{1†}, Quirin Göttl²,
Jakob Burger², Stephan Mandt³, Hans Hasse¹, Fabian Jirasek^{1*}

¹Laboratory of Engineering Thermodynamics, RPTU Kaiserslautern,
Kaiserslautern, Germany.

²Laboratory of Chemical Process Engineering, Technical University of
Munich, Munich, Germany.

³Department of Computer Science & Statistics, University of California,
Irvine, Irvine, CA, USA.

*Corresponding author(s). E-mail(s): fabian.jirasek@rptu.de;

Contributing authors: marco.hoffmann@rptu.de;

thomas.specht@rptu.de; qgctvtum@gmail.com; burger@tum.de;

mandt@uci.edu; hans.hasse@rptu.de;

†These authors contributed equally to this work.

The excess Gibbs energy plays a central role in chemical engineering and chemistry, providing a basis for modeling thermodynamic properties of liquid mixtures. Predicting the excess Gibbs energy of multi-component mixtures solely from molecular structures is a long-standing challenge. We address this challenge with HANNA, a flexible machine learning model for excess Gibbs energy that integrates physical laws as hard constraints, guaranteeing thermodynamically consistent predictions. HANNA is trained on experimental data for vapor-liquid equilibria, liquid-liquid equilibria, activity coefficients at infinite dilution and excess enthalpies in binary mixtures. The end-to-end training on liquid-liquid equilibrium data is facilitated by a surrogate solver. A geometric projection method enables robust extrapolations to multi-component mixtures. We demonstrate that HANNA delivers accurate predictions, while providing a substantially broader domain of applicability than state-of-the-art benchmark methods. The trained model and corresponding code are openly available, and an interactive interface is provided on our website, MLPROP.

1 Introduction

Accurate knowledge of the thermodynamic properties of liquid mixtures is crucial in chemistry, chemical engineering, and environmental science. Among these properties, the molar excess Gibbs energy, g^E , plays a central role: it provides the foundation for deriving many other thermodynamic quantities through established relations. In particular, g^E serves as the basis for determining the activity coefficients of the mixture's components.

Activity coefficients, in turn, govern phase equilibria, such as vapor-liquid (VLE), liquid-liquid (LLE), and solid-liquid (SLE) equilibria, and are key to describing chemical equilibria. They are also used in modeling reaction kinetics and transport phenomena. This makes g^E a central property in model-based process design and optimization. However, g^E and the derived activity coefficients cannot be measured directly but must be inferred from phase equilibrium data, and the corresponding experiments are costly and time-consuming.

Given the many thousands of technically relevant components that can form an enormous number of mixtures, and the fact that g^E depends on the state point (especially temperature and composition in liquid mixtures), only a tiny fraction of all relevant mixtures can be studied experimentally, which makes the development of predictive models for g^E a central task in thermodynamics. We thereby distinguish different classes of predictions, namely, to:

- Unstudied state points: temperatures and/or compositions of a mixture for which data exist at other conditions.
- Unstudied systems: combinations of components for which data exist in other systems.
- Unstudied components: entirely new substances for which no data exist.

All common g^E models are based on the concept of pair interactions. The most widely used g^E models are based on the local-composition theory, such as NRTL [1] and UNIQUAC [2], in which the molecular interactions are described by pair-interaction parameters between components, which are usually fitted to experimental data for each binary system of interest. These models enable predictions for unstudied temperatures and compositions, as well as for unstudied multi-component systems, provided data exist to fit the model parameters of all constituent binary subsystems. However, these models do not allow predictions for unstudied components, binary systems, and multi-component mixtures comprising unstudied binary subsystems. Furthermore, these models suffer from limited flexibility, which often hinders the simultaneous description of VLE and LLE with a single parameterization [3, 4].

To address the lacking capability of predictions to unstudied systems and components, group-contribution (GC) g^E models have been developed, with the different variants of UNIFAC being the most successful ones [5–8]. UNIFAC decomposes components into structural groups and utilizes parameters that describe pair interactions between these groups, significantly reducing the number of parameters and enabling extrapolations to unstudied systems and components. However, models of the UNIFAC family are limited to mixtures for which all involved structural groups (and their interactions) have previously been parametrized. Because the original UNIFAC

model [5] is unable to describe both VLE and LLE with high accuracy, a special UNIFAC parameterization for LLE has been introduced [9]. Additionally, for describing complex systems, such as those containing ionic liquids [10, 11] or formaldehyde [12, 13], tailored groups had to be introduced, compromising the GC nature of UNIFAC and the generality of the approach. Despite the described shortcomings, the different UNIFAC variants have long been and remain the standard g^E models used for the predictive modeling of phase equilibria across industry and academia, when no data for fitting parameters for models such as UNIQUAC and NRTL are available.

An alternative to the GC models of the UNIFAC family are the g^E models based on quantum-chemical density functional theory (DFT) calculations combined with the conductor-like screening model (COSMO) [14]. Different variants of such frameworks have been published, most notably COSMO-RS [15] and COSMO-SAC [16]. While these models avoid group-interaction parameter tables and can, in principle, be applied to any system, they often require expensive calculations, and the results can depend on the chosen DFT level and COSMO parametrization [17–20]. For systems where both approaches can be applied, UNIFAC is often reported to be more accurate than COSMO frameworks [17, 21, 22].

Recently, several authors used machine learning (ML) methods to further extend the scope of physics-based g^E models by predicting their pair-interaction parameters. This was, e.g., done for UNIQUAC [23], NRTL [24], and UNIFAC [25, 26]. These new hybrid methods rely on the established g^E models and are therefore intrinsically thermodynamically consistent. However, these models also inherit all the limitations of the underlying g^E models, e.g., the problems of simultaneously describing VLE and LLE, or the restriction to a predefined list of structural groups [25, 26] or components [23].

Furthermore, several ML models for the prediction of activity coefficients have been proposed that are not based on the equations of any of the physics-based g^E models. Medina et al. presented graph neural network (GNN) architectures for the prediction of infinite-dilution activity coefficients at constant temperature (GNN-IAC) [27], and with temperature dependence (GH-GNN) [28], using the Gibbs-Helmholtz equation. Qin et al. [29] have developed a GNN (SolvGNN) for the prediction of composition-dependent, isothermal activity coefficients in binary and ternary mixtures. Based on the SolvGNN architecture, Rittig et al. have built the Gibbs-Duhem-informed GNN (GDI-GNN) [30] and the excess Gibbs free energy GNN (GE-GNN) [31], which include soft-constraints and hard-constraints on the Gibbs-Duhem equation, respectively.

In recent work, we have introduced HANNA [32], a model that combines the flexibility of artificial neural networks with explicit thermodynamic knowledge hard-coded into the network architecture. In its first version, HANNA was trained on binary activity coefficients derived from experimental VLE data, as well as experimental activity coefficients at infinite dilution (ACI). HANNA is the first model to predict temperature- and composition-dependent activity coefficients without being based on an underlying physics-based g^E model, while still strictly complying with all relevant thermodynamic consistency criteria. These comprise the consistency of the activity coefficients with the Gibbs-Duhem equation, permutation-equivariance (a permutation in the component input order must be equally reflected in the order of the activity coefficients in the output; their values must not change), their correct behavior at

infinite dilution (for $x_i \rightarrow 1, \gamma_i \rightarrow 1$), and consistency for pseudo-mixtures (identical components in the mixture must reduce to one pure component).

In this work, a generalization of HANNA is presented that is flexible enough for the holistic description of different phase equilibria (namely VLE and LLE), enables predictions for multi-component mixtures comprising any number of components, and thereby still strictly complies with all thermodynamic constraints. To achieve this, we significantly improve the training process, which now additionally includes end-to-end training on experimental LLE and excess enthalpy data. Moreover, we implement a geometric projection method for extrapolation to any multi-component mixture. The only input required for HANNA is the molecular structure of the components and the considered state point (temperature and composition). We provide the trained HANNA model to the community in a fully open-source format and also make it available through an intuitive user interface on our website [MLPROP](#).

Fig. 1 gives a high-level overview of HANNA and its training procedure. The network structure of HANNA includes permutation-invariant operations, ensuring that predictions are independent of the order of components in the input, as well as operations that guarantee consistency in the limiting cases of binary subsystems and pure components. To generalize to multi-component mixtures, we introduce a geometric projection method [35] that maps the g_{ij}^E of the binary subsystems into the multi-component space. Because this projection introduces no additional parameters, it is sufficient to train the model only on data from binary mixtures. Details on the HANNA architecture and the projection are given in Section 4.1.

HANNA was trained end-to-end on extensive experimental data sets of binary mixtures, covering activity coefficients (normalized after Raoult’s law) derived from VLE data for which temperature, pressure, and the composition of the liquid and vapor phase are given (TPXY data) and activity coefficients at infinite dilution (ACI data). We also included VLE data for which the vapor-phase composition is unavailable (TPX data) in the training, with total pressure as the training objective. Additionally, we trained to phase compositions from LLE data and excess enthalpies (HE data). All data was taken from the Dortmund Data Bank [39]. The complete data set covers 824,481 data points for 46,543 unique systems of 4114 unique components with a large chemical diversity, also including ionic liquids. Details on the data set can be found in Section 4.2.

To include LLE data into the training process, we developed a new training strategy using a surrogate solver that circumvents the necessity for iteratively solving non-linear equations during training [40]. To the best of our knowledge, this is the first time that experimental phase compositions from LLE data were used in the end-to-end training of an ML-based g^E model. Furthermore, to train HANNA on HE data, we leverage the temperature derivative of the predicted excess Gibbs energy, which is easily available through automatic differentiation. We also introduce a physically inspired ‘Gibbs loss’ that enhances the recognition and description of LLE based on the stability criterion [40]. Additionally, a Lipschitz regularization strategy was employed, increasing HANNA’s robustness outside the training regime by enforcing smoothness of the predicted g^E . Details on the model training are given in Section 4.4.

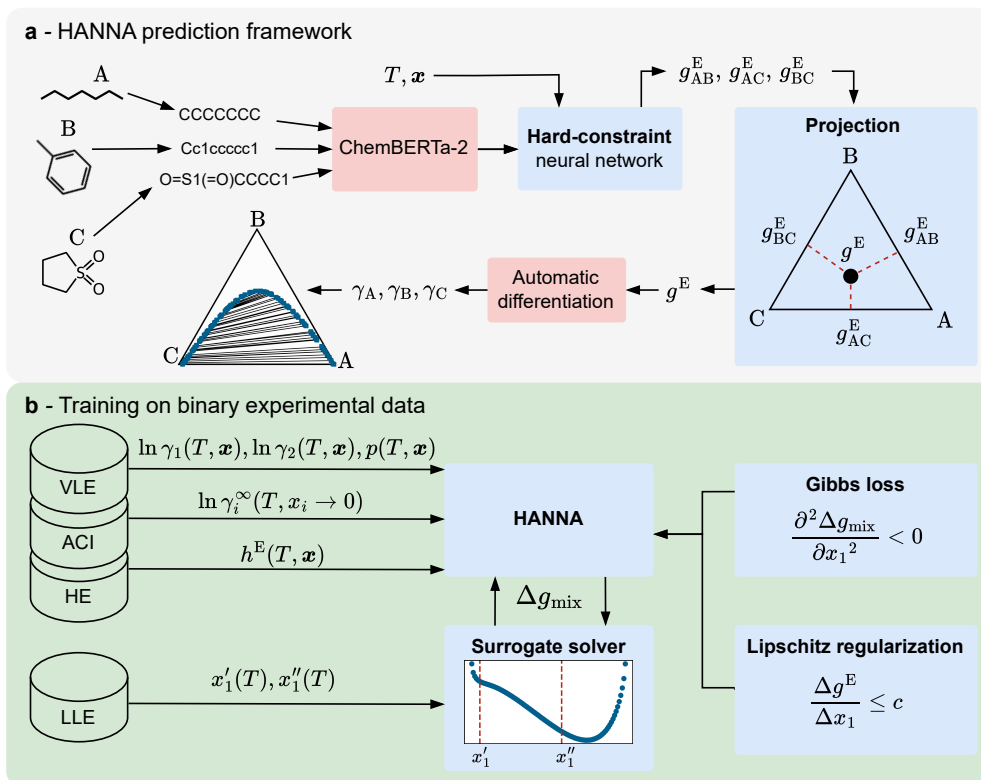


Fig. 1: Overview of the HANNA prediction framework and its training procedure. **a**, As input, HANNA requires the molecular structure of all components in the SMILES [33] notation, the composition of the mixture \mathbf{x} , and the temperature T . In the first step, molecular embeddings are generated from the SMILES using the transformer model ChemBERTa-2 [34]. Subsequently, a hard-constraint neural network that strictly obeys all thermodynamic constraints predicts g_{ij}^E of all binary subsystems, from which g^E in the multi-component mixture is calculated via a geometric projection [35]. Thermodynamically consistent activity coefficients γ_i are obtained by automatic differentiation of g^E and then used to predict phase equilibria using the convex envelope method (CEM) [36–38]. **b**, HANNA is trained on experimental vapor-liquid equilibrium (VLE), liquid-liquid equilibrium (LLE), activity coefficients at infinite dilution (ACI), and excess enthalpy (HE) data of binary mixtures. End-to-end training on the experimental LLE data is enabled by a new surrogate solver using the Gibbs energy of mixing Δg_{mix} . An additional Gibbs loss incentivizes the model to produce negative second derivatives of Δg_{mix} in the LLE regime, and a Lipschitz regularization enforces smoother g^E functions.

In the following, we demonstrate the performance of HANNA for predicting activity coefficients derived from VLE (TPXY data), ACI data, and phase compositions in LLE in binary and ternary mixtures. All results were obtained exclusively on unseen test systems withheld during training HANNA.

2 Results

Comparison to mod. UNIFAC

Figure 2 compares HANNA’s predictive performance for binary mixtures against that of modified UNIFAC (Dortmund) [7, 8], hereafter referred to as mod. UNIFAC. We use mod. UNIFAC as the primary benchmark in this work, because it is the most established predictive g^E model in industry and academia.

The results shown in the boxplots of Fig. 2a demonstrate that HANNA has a higher prediction accuracy than mod. UNIFAC on the shared mod. UNIFAC horizon (i.e., all systems to which mod. UNIFAC could be applied) for all studied data types: activity coefficients from vapor-liquid equilibria data (TPXY, top), activity coefficients at infinite dilution (ACI, middle), and phase compositions in liquid-liquid equilibrium (LLE, bottom). We assess the performance using the system-specific mean absolute error MAE_{sys} , cf. Section 4.5. The most significant difference is found for the ACI data, where the median of MAE_{sys} is reduced from 0.18 (mod. UNIFAC) to 0.11 (HANNA). This substantial improvement could be related to a deficiency of UNIQUAC (on which UNIFAC is based) to correctly predict infinite dilution activity coefficients in strongly non-ideal systems [41].

Beyond the mod. UNIFAC horizon, the performance of HANNA slightly declines for the VLE and LLE data (cf. full horizon), which could be attributed to systems with more complex components containing rarely occurring groups that mod. UNIFAC fails to predict entirely because not enough data were available to regress the required parameters. Importantly, for the LLE data, error scores could only be calculated if the respective model predicts a miscibility gap at the given state point. Therefore, the number of systems for which predictions are obtained differs from the number of systems within the LLE data set that are theoretically feasible with the models. On the mod. UNIFAC horizon¹, mod. UNIFAC correctly identifies miscibility gaps for 74% of the LLE systems, whereas HANNA achieves 89% accuracy. On the full horizon, HANNA correctly identifies miscibility gaps for 83% of the LLE systems.

For the ACI data, the full horizon we evaluate HANNA on contains more than twice as many systems as the mod. UNIFAC horizon. The largest share of the additional systems HANNA predicts here contains at least one ionic liquid (IL). As only very few groups to model ILs have been parameterized within mod. UNIFAC, it has a very limited scope for systems containing ILs, whereas HANNA has no such restrictions. In Fig. S.10 in the Supplementary Information, we specifically evaluate the performance of HANNA for predicting activity coefficients in IL systems and compare it to that of mod. UNIFAC for the few IL systems for which mod. UNIFAC can be used. The results show significantly higher prediction accuracy for HANNA both on the mod. UNIFAC horizon and the full horizon.

Three typical examples for predictions of binary VLE diagrams with HANNA are shown in Fig. 2b. The predictions were obtained using extended Raoult’s law with vapor pressures calculated from the Antoine parameters of the DDB [39]. For all systems, HANNA shows good agreement with the experimental data. HANNA correctly

¹For a fair comparison, the mod. UNIFAC horizon of the LLE data comprises only systems that mod. UNIFAC can model and for which both mod. UNIFAC and HANNA correctly predict a phase split.

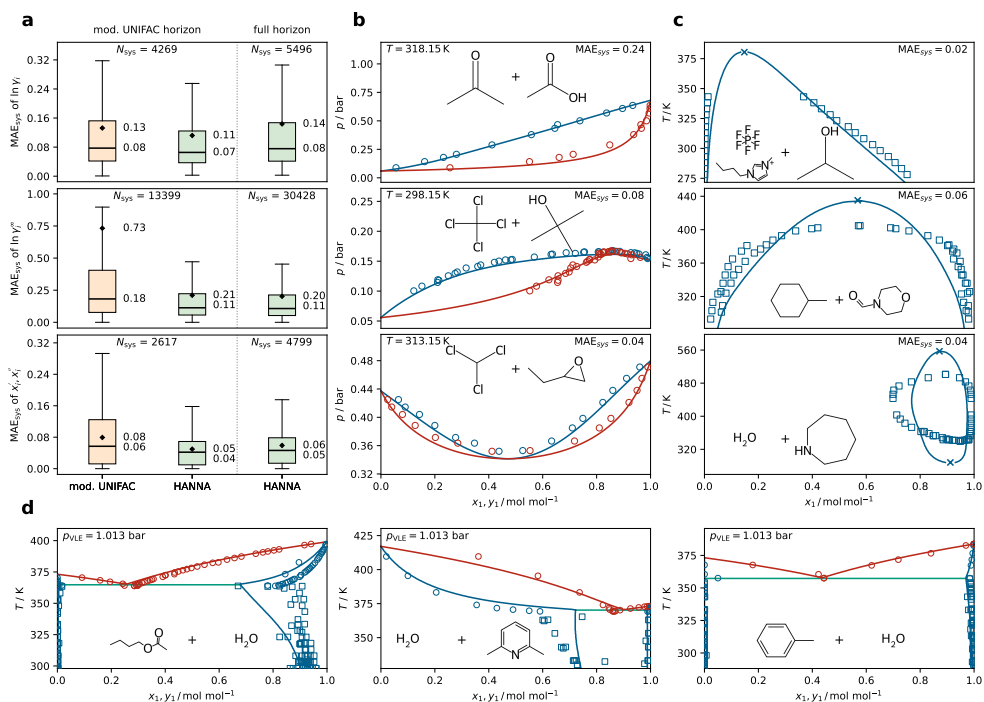


Fig. 2: Predictions for binary mixtures with HANNA.

a, Boxplots comparing the performance of HANNA for predicting activity coefficients in binary VLE (top), ACI (middle), and LLE phase compositions (bottom) with that of mod. UNIFAC in terms of the system-wise mean absolute error MAE_{sys} in $\ln \gamma_i$ (VLE, ACI) or phase compositions x_i' and x_i'' (LLE). For a fair comparison, HANNA was also evaluated only on those systems for which mod. UNIFAC is applicable (mod. UNIFAC horizon). N_{sys} denotes the number of test systems within the respective horizon and data type. The boxes represent interquartile ranges, and the whiskers are 1.5 times the interquartile range. Diamonds mark the mean, horizontal lines the median of the MAE_{sys} values. **b**, Predictions of HANNA for three isothermal VLE plotted against experimental data. Open symbols denote experimental data, and lines are predictions by HANNA. Blue indicates the liquid phase; red indicates the vapor phase. The molecular structures of the components and the respective MAE_{sys} are depicted in the plots; the left molecule corresponds to component 1. **c**, Predictions of HANNA for three LLE. Open squares indicate experimental data, lines represent predictions by HANNA. Predicted upper and lower critical solution temperatures are marked with an 'x'. **d**, Predictions of HANNA for three isobaric heteroazeotropes. Open blue and red circles indicate the experimental liquid and vapor phases, respectively, from VLE data. Open blue squares mark the experimental phase compositions from LLE data; the green line is the vapor-liquid-liquid equilibrium predicted by HANNA. All results shown here are for systems from the test set that were not used for HANNA training.

describes nearly ideal mixtures (top), mixtures with strong negative (middle), and mixtures with strong positive (bottom) deviations from Raoult's law.

Fig. 2c demonstrates that HANNA can also predict different types of LLE phase diagrams. For the predictions, we assume a pressure-independent LLE. As for the ACI data, HANNA also yields good predictions for LLE involving ionic liquids (top), and even correctly qualitatively predicts an island-type miscibility gap with upper and lower critical solution temperatures (bottom).

In Fig. 2d, predictions of HANNA for three heteroazeotropic systems are shown. Both VLE and LLE are well predicted, a task that established g^E models, such as UNIQUAC or NRTL, often only achieve with multiple parameter sets, fitted for different temperature ranges. The results demonstrate HANNA’s applicability across a wide temperature range with a single parameterization. The phase diagrams in Figs. 2c and 2d were obtained using the convex envelope method (CEM) [36–38], which enables a seamless calculation of different types of phase equilibria, considering the global behavior of the studied system, and thus avoiding individual phase equilibrium calculations and the problems associated with this. In Fig. S.8 in the Supplementary Information, we evaluate the predictions of mod. UNIFAC on the systems of Figs. 2b, 2c, and 2d that fall within the mod. UNIFAC horizon.

In Figs. S.6 and S.7 in the Supplementary Information, we compare HANNA and mod. UNIFAC for the prediction of total pressures in binary VLE (TPX data) and binary excess enthalpies (HE data), respectively. For both data types, HANNA yields more accurate predictions than mod. UNIFAC. Additionally, we also compare HANNA to mod. UNIFAC 2.0 [26], a ML-enhanced version of mod. UNIFAC that exceeds the original model in scope due to a completed interaction parameter matrix, and to UNIFAC-LLE [9], a version of UNIFAC that was specifically parameterized to describe LLE data between 283.15 K and 313.15 K. The comparisons to mod. UNIFAC 2.0 and UNIFAC-LLE for binary mixtures are presented in Figs. S.11 and S.14, respectively.

Figure 3 evaluates HANNA’s performance on unseen ternary mixtures. Similar to the results for the binary mixtures, Fig. 3a depicts boxplots of the system-wise MAE for the predictions of activity coefficients in ternary VLE (TPXY, top), infinite dilution activity coefficients in mixed solvents (ACI, middle), and LLE (bottom), and compares the performance of HANNA to that of mod. UNIFAC.

The results in Fig. 3a show higher or equal accuracy of HANNA for the ternary VLE (TPXY) and LLE data compared to mod. UNIFAC within the shared horizon, and a slight decline in the accuracy of HANNA on the full horizon. For the ternary ACI data, we observe slightly higher mean and median values of the MAE_{sys} for HANNA as for mod. UNIFAC. Interestingly, the HANNA scores for ternary ACI data improve when going to the full horizon. On the mod. UNIFAC horizon, mod. UNIFAC correctly identifies the miscibility gaps for 77% of the ternary LLE systems, whereas HANNA achieves 98% accuracy. On the full horizon, HANNA correctly identifies the miscibility gaps for 92% of the systems.

Fig. 3b and Fig. 3c show HANNA predictions for ternary systems exhibiting a VLE or LLE, respectively, and compare them to experimental data. For the LLE prediction, we again neglect the pressure dependence of g^E . Good agreement with the experimental data is found for all four systems. While the results in Fig. 3c cover ternary LLE with one (top) and two (bottom) binary subsystems that exhibit a miscibility gap, LLE examples for systems with complete miscibility of the binary subsystems

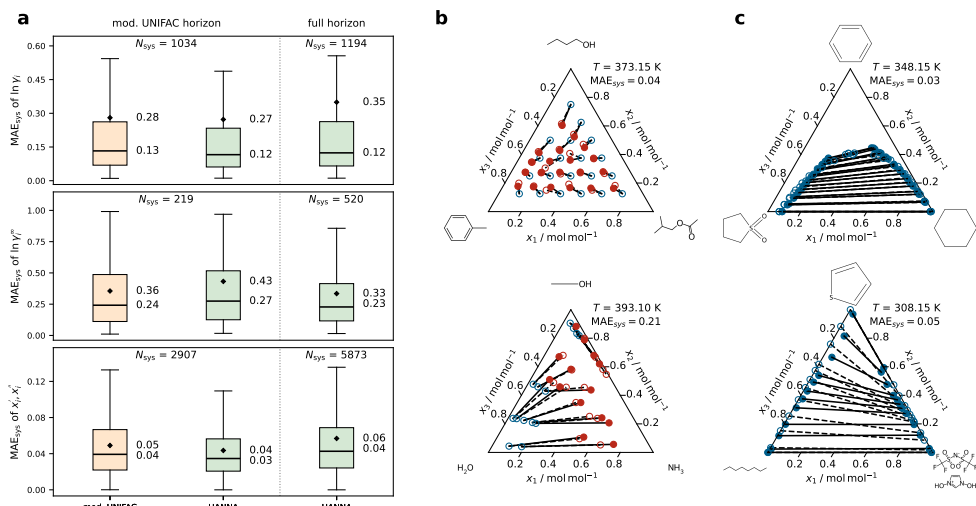


Fig. 3: Predictions for ternary mixtures with HANNA.

a, Boxplots comparing the performance of HANNA for predicting activity coefficients in ternary VLE (top), ACI (middle), and LLE phase compositions (bottom) with that of mod. UNIFAC in terms of the system-wise mean absolute error MAE_{sys} in $\ln \gamma_i$ (VLE, ACI) or phase compositions x_i' and x_i'' (LLE). For a fair comparison, HANNA was also evaluated only on those systems for which mod. UNIFAC is applicable (mod. UNIFAC horizon). N_{sys} denotes the number of test systems within the respective horizon and data type. The boxes represent interquartile ranges, and the whiskers are 1.5 times the interquartile range. Diamonds mark the mean, horizontal lines the median of the MAE_{sys} values. **b**, Predictions of HANNA for two isothermal VLE. Open blue and red symbols mark the experimental liquid and vapor phase compositions, respectively; filled red symbols are the predicted vapor phase compositions. The molecular structures of the components and the respective MAE_{sys} values are also depicted. **c**, Predictions of HANNA for three isothermal LLE. Open symbols and dashed tie lines represent the experimental data; filled symbols and solid lines represent predictions by HANNA. All results shown here are for systems from the test set that were not used for HANNA training.

(island-type LLE behavior) and miscibility gaps in all three binary subsystems (leading to a three-phase LLE) are given in Fig. S.5 in the Supplementary Information. HANNA is also able to predict these correctly, at least qualitatively. Again, we have also compared HANNA against mod. UNIFAC 2.0 and UNIFAC-LLE, which yielded results similar to those against mod. UNIFAC shown here, cf. Figs. S.12 and S.14 in the Supplementary Information, respectively.

Comparing HANNA's performance on binary and ternary mixtures reveals how different extrapolation strategies influence accuracy across VLE, ACI, and LLE data (cf. panels **a** in Figs. 2 and 3). For the ternary VLE data, the scores from HANNA and mod. UNIFAC become slightly worse by the same margin (their median MAE_{sys} increases by about 0.05), compared to the respective binary scores. We observe a similar pattern for the LLE data. For the ACI data, we observe a significant deterioration

in prediction accuracy when moving from binary to ternary mixtures for HANNA (the median MAE_{sys} increases by 0.16).

The extrapolation from binary to multi-component data in mod. UNIFAC is based on the physical lattice model, which uses the pair-interaction concept. In contrast, HANNA uses a purely geometric projection method. To determine whether the projection method is responsible for the deterioration in HANNA for ternary ACI data, we conducted the following test: for all systems in the ternary VLE (TPXY) and ACI data sets, we predicted the corresponding activity coefficient curves for all binary subsystems at the respective temperatures using HANNA. We then fitted two component-specific physics-based g^E models, namely UNIQUAC (the parent model of UNIFAC) and NRTL, to the predicted activity coefficients and used the resulting parameters to predict activity coefficients in the ternary systems. This procedure allows comparison only of the physics-based model extrapolations (UNIQUAC, NRTL) with the geometric extrapolation of HANNA, using the same binary data. The results of this comparison, which are shown in Figs. S.15 and S.16 in the Supplementary Information, indicate a similar or even slightly better accuracy using the geometric projection compared to the extrapolation of the physics-based models. Hence, the geometric Muggianu projection method in the HANNA architecture generally works reasonably well. This is also supported by Fig. S.9 in the Supplementary Information, where we provide a comparison of HANNA and mod. UNIFAC on quaternary VLE and LLE data, showing comparable accuracy of both methods. Nonetheless, this does not exclude that further improvements can be made on the geometric extrapolation, for which different suggestions exist in the literature [42, 43].

The shown results demonstrate that HANNA is a strong competitor to mod. UNIFAC, the most established model for predicting activity coefficients in industry and academia, both for binary and multi-component mixtures. This is especially remarkable because we have evaluated HANNA on data from the DDB, the largest factual database for thermodynamic properties, which is managed essentially by the same group that has revised mod. UNIFAC over several decades. Consequently, we must assume that mod. UNIFAC has been fitted to a significant part of our test data (although the concrete training data for mod. UNIFAC has not been fully disclosed). Similar arguments hold for mod. UNIFAC 2.0 and UNIFAC-LLE. In contrast, the results of HANNA have been obtained on test data, strictly withholding all available data types for the test systems during model training. Hence, most comparisons we have shown here are biased in favor of mod. UNIFAC. In addition to its strong predictive performance, HANNA offers a much broader applicability than mod. UNIFAC, because it can, in principle, be applied to any mixture for which the molecular structures of the components are known; remaining limitations are discussed in the section "Limitations" below.

Comparison to other machine learning models

In the following, we also compare HANNA against different ML models from the literature. We thereby consider only ML models that, like HANNA, are not based on the equation framework of a physics-based g^E model, require only the SMILES of the components as input, and for which the model parameters are disclosed or can be

reproduced with the available code. Specifically, we have selected GE-GNN [31], GDI-GNN [30], SolvGNN [29], and GNN-IAC [27] as additional benchmarks. Compared to HANNA, all these models have limitations in their applicability: they are only applicable to binary systems (GE-GNN, GDI-GNN, GNN-IAC), to the state of infinite dilution (GNN-IAC), or to predictions at $T = 298$ K (all). Furthermore, they lack strict consistency with the Gibbs-Duhem equation (GDI-GNN, SolvGNN) or in the limiting case of pure components (GE-GNN, GDI-GNN, SolvGNN), whereas HANNA complies with all relevant constraints. Tab. S.2 in the Supplementary Information summarizes the ranges of applicability of these models and the consistency criteria they comply with.

For a fair comparison, we evaluate HANNA and the other ML models on common subsets of our data for which predictions are feasible with all models. While the results of HANNA on these subsets are true predictions (since the respective systems were not part of the training or validation sets), we cannot rule out that some of them were included in the training sets of the literature models. We note that GE-GNN, GDI-GNN, and SolvGNN have not been trained on experimental data but on synthetic data generated with COSMO-RS [15].

Table 1: Comparison of HANNA with different ML models from the literature. We evaluate all models (including HANNA) only on isothermal data at 298 K and exclude all systems containing ionic liquids from the comparison. Because the architecture of GNN-IAC is not suited to processing water, systems that contain water are omitted from the binary ACI comparison. The mean and median of the MAE_{sys} for each data type are given. The best scores for each data type are bold. The results for HANNA are for test data; the other models were used as published.

	Model	TPXY		TPX		ACI		LLE	
		Mean	Median	Mean	Median	Mean	Median	Mean	Median
Binary	HANNA	0.165	0.066	0.151	0.050	0.229	0.141	0.032	0.011
	GE-GNN	0.227	0.108	0.272	0.091	0.438	0.296	0.051	0.012
	GDI-GNN	0.225	0.109	0.278	0.090	0.433	0.288	0.046	0.009
	SolvGNN	0.225	0.109	0.280	0.091	0.432	0.293	₋₃	₋₃
	GNN-IAC	₋₄	₋₄	₋₄	₋₄	0.372	0.150	₋₄	₋₄
Ternary	HANNA	0.646	0.143	0.310	0.141	0.429	0.257	–	–
	SolvGNN	0.689	0.189	0.667	0.328	0.841	0.758	₋₃	₋₃

³Due to large oscillations in the predicted activity coefficients over the concentration, SolvGNN could not be evaluated on LLE data.

⁴GNN-IAC can only predict activity coefficients at infinite dilution.

The results of the comparison are summarized in Tab. 1. The scores of GE-GNN, GDI-GNN, and SolvGNN on the binary TPXY, TPX, and ACI data are almost identical, which could be expected, as all three models rely on the same GNN architecture and training data set and only differ in the final step of the prediction of the activity coefficients and/or the regularization during training. In fact, the authors arrived at a similar conclusion when comparing GE-GNN against GDI-GNN and SolvGNN on their extrapolation test data set [31]. For the TPXY, TPX, and ACI data, HANNA shows significantly lower scores (higher accuracy) for both binary and ternary systems. On the LLE subset, HANNA achieves the lowest mean MAE_{sys} , suggesting the fewest outliers, while no significant difference in the median MAE_{sys} between the models is observed. Overall, HANNA shows the best performance, with the highest prediction accuracy in almost all cases and a significantly broader applicability than all benchmark models, cf. Tab. S.2 in the Supplementary Information.

Limitations

We have demonstrated that HANNA provides accurate predictions for activity coefficients in binary and ternary mixtures, and that phase equilibria calculated from these predictions agree well with experimental data. The training data used here consists of VLE (TPXY and TPX), ACI, LLE, and HE data, with 95% in a temperature range between 273 K and 428 K. Similar to other g^E models, HANNA can also be used to predict activity coefficients for phase equilibria with supercritical components (using Henry’s law) or solid-liquid equilibria (SLE). However, HANNA’s performance on these additional data types and outside the described temperature range is yet to be evaluated. Furthermore, HANNA, like most g^E models, neglects the pressure dependence of the liquid phase activity coefficients. While this is a valid assumption for most engineering applications, it may break down at very high pressures.

HANNA was trained on a large, diverse dataset and has learned to accurately predict activity coefficients for mixtures of components from many classes, including both small and large molecular components and components containing exotic chemical groups. Weak electrolytes that may dissociate partially and ionic liquids were also included in the training set and are therefore within the current scope of HANNA. However, HANNA does not treat ions explicitly. Instead, any effects of dissociation are implicitly embedded in the binary training data. The extension to explicit modeling of the ionic species is beyond the scope of this work. Also, data on polymers were not considered, so HANNA should not be used for polymer systems (note that this is currently also not possible for technical reasons, as ChemBERTa-2 does not support the correct conversion of SMILES into embeddings for molecules consisting of more than 512 tokens [34, 44]). Furthermore, HANNA was not trained on solutions of strong electrolytes (except ionic liquids), so that HANNA should not be used for these systems.

In the extensive tests we have conducted, HANNA consistently produced activity coefficients that yielded plausible phase behavior. The only exception to this was a small fraction (<1%) of the binary LLE systems, for which we found that HANNA predicts the existence of two separate LLE phase regions at elevated temperatures.

Although this is thermodynamically possible, it has, to our knowledge, not been experimentally observed in these systems. Most of the affected systems contain methanol, ethanol, or water. We speculate that the ChemBERTa-2 [34] tokenization for methanol (SMILES: 'CO') and ethanol (SMILES: 'CCO') into 'C' (equivalent to the SMILES for methane) and 'O' (equivalent to the SMILES for water) results in embeddings that cannot fully capture the properties of these small molecules. In the future, this could be overcome by introducing a distinct token for methanol and/or water; a similar strategy was used in mod. UNIFAC, which has dedicated groups for methanol and water. Despite the fundamentally different architecture and training data, we observe a similar behavior for predictions from GE-GNN, where some systems containing methanol or water are also affected. Note that Antolović et al. [45] have recently encountered similar anomalies for predictions of LLE with COSMO-SAC.

While the Lipschitz regularization promotes the smoothness of the HANNA predictions with respect to a variation of the inputs (components, temperature, and composition), excessively strong regularization overly restricts the model's flexibility and reduces its predictive performance. With the chosen regularization, HANNA, in some cases, exhibits small fluctuations of the predicted activity coefficients with respect to the composition. Because this only affects nearly ideal mixtures, i.e., with very small activity coefficients, it does not compromise HANNA's practical applicability.

3 Discussion

This work presents HANNA, a ML-based g^E model that enables the thermodynamically consistent prediction of activity coefficients in liquid mixtures with an arbitrary number of components solely from the chemical formula of the constituent components. HANNA was trained on a large, diverse data set for vapor-liquid equilibria (VLE), activity coefficients at infinite dilution (ACI), excess enthalpies (HE), and liquid-liquid equilibria (LLE), resulting in a model with broad applicability.

The results of HANNA were systematically compared to those from state-of-the-art models from the UNIFAC family and other ML-based models from the literature for binary and ternary mixtures, overall demonstrating a better performance of HANNA - despite an important bias of the comparison in favor of the benchmark models: while all results for HANNA were true predictions (none of the systems in our test set was used for training HANNA), this is not true for the other models, for which we must assume that many of the systems in the test set were also used for the training. Even more importantly, HANNA has much broader applicability than UNIFAC, as only the component SMILES are required, which are always available. Similarly, HANNA is much more broadly applicable than all other ML-based models in the literature, which are, among others, restricted to a single temperature.

HANNA is the first g^E model in which the entire relevant thermodynamic knowledge is embedded in a neural network as hard constraints. It therefore fully leverages the flexibility of neural networks, but applies it only within the bounds permitted by physical principles. This flexibility enables HANNA to simultaneously describe VLE and LLE with high accuracy with a single parameterization.

A ready-to-use version of HANNA, trained on all available data for binary mixtures (including the data retained as test data for the comparison in the present work), is available on [GitHub](#). Furthermore, we also provide an interactive interface for HANNA on our website [MLPROP](#). We encourage users to give us feedback.

Several enabling technologies used within the work on HANNA merit to be highlighted, as they are useful far beyond the work described here: 1) Based on the convex envelope method (CEM), we have developed a new surrogate solver for determining LLE phase compositions that can be incorporated in the workflow of ML model training. 2) Using the CEM to determine LLE, we have obtained phase-split predictions in a numerically robust and initialization-independent manner for thousands of systems in an automated workflow. Unlike conventional solvers, the CEM does not require careful initialization or phase-stability checks to identify the correct number of coexisting phases. 3) By applying a geometric projection method, a model for predicting properties of binary mixtures can be seamlessly extended to multi-component mixtures without the need for additional parameters.

HANNA represents a major advancement in predicting the thermodynamic properties of liquid mixtures. Because we release both the full model architecture and trained parameters as open source, process engineers can integrate HANNA directly into existing workflows and simulation software. Users who prefer to continue to use conventional thermodynamic models can, e.g., fit NRTL or UNIQUAC parameters to HANNA’s predictions. These fitted parameters can directly be used in established simulation frameworks without additional implementation effort, albeit typically with some loss in accuracy relative to the original HANNA predictions. A routine for fitting NRTL parameters to HANNA is also provided in MLPROP. Additionally, HANNA is interesting for material design, e.g., for identifying promising solvents for chemical reactions and separation processes like extraction, extractive distillation, absorption, and crystallization.

The current version of HANNA is already a widely applicable and accurate g^E model that outperforms current state-of-the-art benchmark models. To further extend the scope of HANNA, we plan to address the following aspects:

So far, we have used data from measurements of VLE, ACI, LLE and HE for training HANNA. In future work, data on solid-liquid equilibria (SLE) could also be included. These data would extend the training data’s temperature range at its lower end [46]. Moreover, only binary data have been used for training HANNA, and the g^E for multi-component mixtures is found by a geometric projection of the g^E of all constituent binary subsystems. In future work, new projection strategies could be developed for this purpose and it could be considered to include ternary data in the fitting process. This has a bad reputation for parameterizing physics-based g^E models, but it could be worth testing the option for hybrid models like HANNA. Even the introduction of ternary parameters could be considered.

HANNA currently uses the pre-trained transformer model ChemBERTa-2 [34] to obtain the molecular embeddings from SMILES strings. ChemBERTa-2 was trained on a wide range of basic chemical data [34] and could be fine-tuned for the present application; however, this would significantly increase the computational cost of training

without guaranteeing better results. As described above, we have observed minor deficiencies that are likely associated with issues of ChemBERTa-2 and may be resolved by a workaround within ChemBERTa-2, without the need for a complete revision. Specifically, one of the unused tokens in ChemBERTa-2 could be assigned to the water molecule, such that water and, e.g., hydroxyl groups no longer share the same token. Another option would be to provide different molecular embeddings, e.g., based on the SELFormer [47] that uses SELFIES [48] instead of SMILES or even use learnable embeddings from a graph neural network [49].

Last but not least, we look forward to user feedback, which we will gladly use to further improve HANNA in ways we may not yet have anticipated.

4 Methods

4.1 HANNA architecture

Algorithm 1 explains the forward pass of the HANNA architecture, starting with the molecular embeddings, the temperature, and the composition of an arbitrary N -component mixture of interest as input and providing predictions for the molar excess Gibbs energy of the mixture and the activity coefficients of the N components in the mixture as output.

Algorithm 1 Forward pass of HANNA. The HANNA architecture is implemented in *PyTorch* [50].

Input: temperature T , mole fractions $\mathbf{x} = [x_1, \dots, x_{N-1}]$, molecular ChemBERTa-2

embeddings $\mathbf{E} = [e_1, \dots, e_N]$

- 1: $T^* = \text{Temperature_Scaler}(T)$, $e_i^* = \text{Embedding_Scaler}(e_i)$ ▷ Scale inputs
- 2: $x_N = 1 - \sum_{i=1}^{N-1} x_i$ ▷ Calculate x_N via summation condition
- 3: $\theta_i = \text{Embedding_Network}(e_i^*)$ ▷ Refine molecular embeddings
- 4: $R_{ij} = \exp(-\gamma \|\theta_i - \theta_j\|^2)$ with $\gamma = 100$ ▷ Compute component similarity score
- 5: $\tilde{x}_i = \sum_{j=1}^N x_j R_{ij}$ ▷ Lump identical components, cf. Eq. (2)
- 6: **for all** $1 \leq i < j \leq N$ **do** ▷ Loop over all $K = N(N-1)/2$ binary subsystems
- 7: $X_i^{(ij)} = \frac{1 + \tilde{x}_i - \tilde{x}_j}{2}$; $X_j^{(ij)} = \frac{1 + \tilde{x}_j - \tilde{x}_i}{2}$ ▷ Muggianu projection, cf. Eq. (1)
- 8: $\mathbf{c}_i^{(ij)} = [\theta_i, X_i^{(ij)}, T^*]$; $\mathbf{c}_j^{(ij)} = [\theta_j, X_j^{(ij)}, T^*]$
- 9: $\alpha_i^{(ij)} = \text{Mixture_Network}(\mathbf{c}_i^{(ij)})$; $\alpha_j^{(ij)} = \text{Mixture_Network}(\mathbf{c}_j^{(ij)})$
- 10: $\phi_{ij} = \text{Property_Network}(\alpha_i^{(ij)} + \alpha_j^{(ij)})$ ▷ Compute binary interactions
- 11: $q_{ij} = \phi_{ij}(1 - R_{ij})$ ▷ Enforce consistency for pure components
- 12: $\frac{g^E}{RT} = \sum_{i=1}^{N-1} \sum_{j=i+1}^N x_i x_j q_{ij}$ ▷ Compute g^E as weighted sum, cf. Eq. (3)
- 13: $\ln \gamma_i = \frac{g^E}{RT} + \frac{\partial}{\partial x_i} \left(\frac{g^E}{RT} \right) - \sum_{j=1}^{N-1} x_j \frac{\partial}{\partial x_j} \left(\frac{g^E}{RT} \right)$
- 14: $\ln \gamma_N = \frac{g^E}{RT} - \sum_{j=1}^{N-1} x_j \frac{\partial}{\partial x_j} \left(\frac{g^E}{RT} \right)$
- 15: **return** $(\ln \gamma = [\ln \gamma_1, \dots, \ln \gamma_N], \frac{g^E}{RT})$

The input of HANNA contains the numerical molecular embeddings e_i of the N components that make up the mixture to be modeled, summarized in $\mathbf{E} = [e_1, \dots, e_N]$, which are calculated individually with the transformer-based model ChemBERTa-2 from the respective component’s SMILES (canonized with RDKit [51]). We use the

'77M-MTR' variant of ChemBERTa-2 from Hugging Face [44] with a slightly corrected tokenizer [32]. Additionally, HANNA requires the temperature T and the mole fractions x_1, \dots, x_{N-1} of $N-1$ components as input. The HANNA architecture comprises three feed-forward neural networks (FFNN), namely, the `Embedding_Network`, the `Mixture_Network`, and the `Property_Network`. The `Embedding_Network` consists of one layer, while the other two networks consist of two layers. In all cases, we use the Sigmoid Linear Unit (SiLU) activation function.

All layers are modified linear layers with 96 nodes (except for the input layer of the `Mixture_Network`, which consists of 98 nodes as the temperature and the projected mole fraction of the respective component are concatenated to the output of the `Embedding_Network`) to which a Lipschitz regularization (cf. Section 4.4) is applied. HANNA computes the molar excess Gibbs energy for the N -component mixture of interest through a geometric projection from the binary subsystems [42, 43, 52–54]. For this purpose, the mole fractions of the N -component mixture are projected onto all $N(N-1)/2$ binary subsystems (cf. loop starting in step 6 of Algorithm 1). In this work, we use the Muggianu projection [35], which, unlike other projection methods, does not exhibit singular points at infinite dilution [55, 56]. The projected mole fractions X_i^{ij} and X_j^{ij} in the binary subsystem i - j are given by:

$$X_i^{(ij)} = \frac{1 + \tilde{x}_i - \tilde{x}_j}{2} \quad \text{and} \quad X_j^{(ij)} = \frac{1 + \tilde{x}_j - \tilde{x}_i}{2} \quad (1)$$

whereby \tilde{x}_i and \tilde{x}_j are the corrected mole fractions of component i and j respectively (cf. below). The projection strictly fulfills the summation condition in each binary subsystem, i.e., $X_i^{(ij)} + X_j^{(ij)} = 1$. Furthermore, if a binary mixture is studied, the projected mole fractions reduce to the corrected mole fractions, i.e., $X_i^{(ij)} = \tilde{x}_i$ and $X_j^{(ij)} = \tilde{x}_j$, ensuring a consistent transition of the HANNA predictions going from binary to a multi-component mixture. In contrast to the original publication [35], we correct the original mole fractions x_i in the N -component mixture before the projection as follows (cf. step 4 and 5 in Algorithm 1):

$$\tilde{x}_i = \sum_{j=1}^N x_j R_{ij} \quad \text{with} \quad R_{ij} \in [0, 1] \quad (2)$$

With this correction, we lump identical components, indicated by a component similarity score $R_{ij} = 1$, into a single component, thereby ensuring that, e.g., for a system of three components A, B, and C, where B is identical to C, the exact same results are obtained as for the binary system of A and B (when accounting for the lumped mole fractions). To compute the component similarity score R_{ij} , we apply the radial basis function (RBF) on pairs of the refined molecular embeddings. By setting the hyperparameter γ of the RBF to the high value of 100, we ensure that only extremely similar components result in a similarity score of $R_{ij} = 1$, so only components that we consider truly identical are lumped together.

Finally, the molar excess Gibbs energy g^E of the N -component mixture is calculated as follows [43]:

$$\begin{aligned} \frac{g^E}{RT} &= \frac{1}{RT} \sum_{i=1}^{N-1} \sum_{j=i+1}^N \frac{x_i x_j}{X_i^{(ij)} X_j^{(ij)}} g_{ij}^E(X_i^{(ij)}, X_j^{(ij)}) \\ &= \sum_{i=1}^{N-1} \sum_{j=i+1}^N x_i x_j q_{ij}(X_i^{(ij)}, X_j^{(ij)}) \end{aligned} \quad (3)$$

where g_{ij}^E is the molar excess Gibbs energy of the binary subsystem i - j and q_{ij} is the learned binary interaction between component i and j in the respective binary subsystem. q_{ij} is calculated using a deep set architecture [57] including a summation aggregation (cf. step 10 in Algorithm 1) to ensure the permutation invariance of the predicted molar excess Gibbs energy, i.e., to ensure that the order of the components in the input of HANNA does not influence its results. For technical reasons, namely, to prevent divisions by zero in Eq. (3) if one of the projected mole fractions approaches zero, we directly predict the binary interaction term q_{ij} with HANNA for each binary subsystem in the projected space (cf. step 11 in Algorithm 1). Here, again, the component similarity score R_{ij} is used, ensuring thermodynamically sound predictions by enforcing $q_{ij} = 0$ and, ultimately, $g_{ij}^E = 0$ for identical components i and j . Using the Autograd functionality of *PyTorch*, the activity coefficients for all N components are finally derived from g^E of the N -component mixture (cf. steps 13 and 14 in Algorithm 1), ensuring strict Gibbs-Duhem consistency [58].

4.2 Data

The experimental data used to train and evaluate HANNA in this work were taken from the 2025 version of the Dortmund Data Bank (DDB) [39]. Data points labeled as poor quality by the DDB’s internal criteria were excluded. Furthermore, only components for which a canonical SMILES string could be generated with RDKit [51] using mol-files from the DDB were considered. Tab. 2 gives an overview of the final data sets of the different data types for binary, ternary, and quaternary systems. A detailed description of each data type is given below.

Vapor-liquid equilibrium data

Two types of experimental VLE data were used in this work: On the one hand, we considered data points in the DDB [39] that contain all information on temperature, pressure, as well as liquid and vapor phase compositions. These are labeled as TPXY data. From the TPXY data, activity coefficients for all components i were calculated with the extended Raoult’s law:

$$\gamma_i = \frac{p y_i}{p_i^s x_i}, \quad (4)$$

where γ_i is the activity coefficient of component i normalized according to Raoult’s law in the mixture, x_i and y_i are the mole fractions of component i in the liquid and vapor phase in VLE, respectively, p denotes the total pressure, and p_i^s is the pure-component vapor pressure of i at the same temperature as the VLE data. The pure-component vapor pressures were computed using the Antoine equation with coefficients from the DDB [39]. On the other hand, we used VLE data that does not include information on the composition of the vapor phase. Consequently, these are labeled as TPX data. Because activity coefficients cannot be calculated for the TPX data, we use total pressure as the training objective for those data points. By using extended Raoult’s law for all VLE data points in our work, we assume that the vapor phase can be treated as an ideal gas mixture and that the pressure dependence of the chemical potential in the liquid phase can be neglected. To justify these assumptions, all TPXY and TPX data points with pressures higher than 10 bar were excluded.

Activity coefficients at infinite dilution

Activity coefficients at infinite dilution γ_i^∞ normalized according to Raoult’s law, called 'ACI' throughout this work, were considered for binary and ternary mixtures. For binary mixtures, i.e., with pure solvents, these data could be used directly. For the activity coefficients at infinite dilution in mixed solvents, we observed several errors in the DDB, mostly interchanged solvent labels, so that these data had to be curated prior to use. Our detailed data curation protocol is described in section "Data curation of activity coefficients at infinite dilution in mixed solvents" in the Supplementary Information.

Liquid-liquid equilibrium data

The LLE data in the DDB contains information on the temperature T and the mole fractions in the coexisting phases x'_i and x''_i (and x'''_i in the case of a three-phase equilibrium). Here, data for binary, ternary, and quaternary mixtures were considered. For binary data, we followed the notation of the DDB and defined the phase compositions such that x'_1 is always the phase composition with the lower value, i.e., $x''_1 > x'_1$ always holds, which is important for training the surrogate solver, cf. Section 4.3. Only for roughly a quarter of the LLE data points in the DDB are all phase compositions specified at the specified temperature. For the remaining data points, only the composition of one phase is available. Nonetheless, we included these data points in our dataset. Because HANNA does not consider the pressure dependence of the excess Gibbs energy and thus the activity coefficients, we excluded all LLE data points with pressures above 50 bar.

Excess enthalpies

Finally, we also extracted experimental data for the excess enthalpies h^E of binary and ternary mixtures from the DDB. Each data point consists of the temperature T , the mole fraction x_1 , and the excess enthalpy h^E .

Table 2: Overview of the final data sets used in this work. All data were taken from the DDB [39].

	Data set	Data points	Systems	Components
Binary	TPXY	193 484	5496	985
	TPX	174 409	4885	1005
	ACI	124 058	30 428	2229
	LLE	76 041	5787	2330
	HE	256 489	9574	1347
Ternary	TPXY	43 021	1194	374
	TPX	20 326	448	252
	ACI	5832	520	133
	LLE	89 961	6407	1413
	HE	31 455	662	211
Quaternary	VLE	3763	132	87
	LLE	19 255	1036	340

Data splitting and scaling.

Following a cross-validation approach, we randomly split the data sets for binary mixtures system-wise into ten folds, each representing a mutually exclusive test set of 10 % of the binary systems. A stratified split strategy was employed, such that the share of each data type is roughly equal for all folds. The remaining data (90 % of the systems) of each fold were again split system-wise into a training set (90 %) and a validation set (10 %). In the data splits, all types of data for a particular system were put exclusively within a single set; for instance, if LLE data for a particular system were in the test set, all TPXY, TPX, ACI, and HE data for this system were also in the test set. This strategy enabled the use of all available data as unseen test data for the evaluation of HANNA.

Furthermore, an additional data split was carried out, where 95 % of the binary systems were used in the training set and 5 % in the validation set (i.e., no test set was withheld). This split, denoted as 'full data split' in the following, was used to train the model that was subsequently evaluated on the data for ternary and quaternary systems and is also deployed as the 'final model' with this work.

The molecular embeddings from ChemBERTa-2, as well as the temperature, were scaled using the *scikit-learn* [59] `StandardScaler()`. Individual scalers were fitted to each training data set to prevent any information leakage.

4.3 Surrogate LLE Solver

From the binary TPXY data points, activity coefficients can be calculated directly using the extended Raoult's Law, cf. Eq. (4). Hence, the training of HANNA on these data is straightforward using a loss function for the predicted activity coefficients, cf. Section 4.4. In contrast, it is not possible to explicitly calculate activity coefficients from the binary experimental LLE data. Using HANNA, one could obtain phase compositions for a given system and state point using iterative solvers [40] and compare to

experimental data. However, integrating iterative solvers into a deep learning framework is tedious because gradients are not easily trackable and, moreover, it would significantly slow down the training process. To overcome this, we developed a differentiable surrogate solver to estimate the binary LLE phase compositions resulting from the activity coefficients predicted by HANNA. This surrogate solver is realized by a feed-forward neural network that mimics the convex envelope method (CEM) [36–38] and maps a discretized graph of the scaled molar Gibbs energy of mixing

$$\frac{\Delta g_{\text{mix}}}{RT} = x_1 \ln(x_1 \gamma_1) + x_2 \ln(x_2 \gamma_2) \quad (5)$$

onto the compositions of the two coexisting liquid phases x'_1 and x''_1 . During the training of HANNA, the surrogate solver allows the model to directly learn from experimental LLE data while maintaining full compatibility with gradient-based optimization. The architecture and training process of the surrogate solver are described in the following.

As input, the surrogate solver gets a vector of $\Delta g_{\text{mix}}/RT$ values calculated with HANNA at 101 uniformly spaced discrete compositions from $x_1 = 0$ to $x_1 = 1 \text{ mol mol}^{-1}$ at constant temperature T . The $\Delta g_{\text{mix}}/RT$ values from HANNA are then processed through three fully connected layers with a hidden size of 64, each followed by the Rectified Linear Unit (ReLU) activation function. The output layer yields two values that correspond to x'_1 and x''_1 (we always define x'_1 as the phase composition with the lower value, cf. Section 4.2), which are subsequently processed through a sigmoid function to constrain the mole fractions between 0 and 1. To align with the demand of thermodynamic consistency of the model, the surrogate solver must be permutation-equivariant with respect to the order of the molecules in the input, i.e., if the discretized Gibbs energy of mixing is given in reverse order, it must yield $1 - x''_1$ and $1 - x'_1$. To enforce this, upon calling the forward function of the surrogate solver with a discretized $\Delta g_{\text{mix}}/RT$ vector, the phase compositions are calculated twice, both from the original vector and the reversed vector. The two values obtained for x'_1 and x''_1 are then averaged. Besides guaranteeing permutation-equivariance, this procedure also prevents any bias in the order of the training data from negatively impacting the training.

The surrogate solver was trained only on synthetic data, namely, predictions of $\Delta g_{\text{mix}}/RT$ obtained with mod. UNIFAC. More specifically, for every experimental LLE data point in our data set within the mod. UNIFAC horizon, we calculated $\Delta g_{\text{mix}}/RT$ for the 101 discrete uniformly spaced compositions at the temperature of the respective data point with mod. UNIFAC. We then used the CEM to determine the corresponding phase compositions, which served as the training objective of our surrogate solver. If no phase split was found, the data point was dropped. We used the same system-wise split as for the experimental data (cf. Section 4.2) to split the synthetic surrogate solver data into training, validation, and test sets. This prevents information leakage through the surrogate solver when training HANNA. Detailed results of the surrogate solver training are provided in the section "Surrogate solver" in the Supplementary Information, along with an example of its functionality given in Fig. S.1.

4.4 Training of HANNA

HANNA was trained by minimizing the total loss $\mathcal{L}_{\text{total}}$ defined as:

$$\mathcal{L}_{\text{total}} = \frac{1}{N_b} \left(\mathcal{L}_{\text{TPXY}} + w_{\text{TPX}} \mathcal{L}_{\text{TPX}} + \mathcal{L}_{\text{ACI}} + w_{\text{LLE}} \mathcal{L}_{\text{LLE}} \right. \\ \left. + w_{\text{HE}} \mathcal{L}_{\text{HE}} + w_{\text{Gibbs}} \mathcal{L}_{\text{Gibbs}} + w_{\text{Lips}} \mathcal{L}_{\text{Lips}} \right) \quad (6)$$

where N_b is the batch size, $\mathcal{L}_{\text{TPXY}}, \mathcal{L}_{\text{TPX}}, \mathcal{L}_{\text{ACI}}, \mathcal{L}_{\text{LLE}}, \mathcal{L}_{\text{HE}}$ are the individual data losses, $\mathcal{L}_{\text{Gibbs}}$ is the Gibbs loss, $\mathcal{L}_{\text{Lips}}$ is the Lipschitz regularization, and $w_{\text{TPX}}, w_{\text{LLE}}, w_{\text{HE}}, w_{\text{Gibbs}}, w_{\text{Lips}}$ are the corresponding weight factors that were determined in a hyperparameter grid search, cf. section "Grid search" in the Supplementary Information for details.

Data Losses

In the individual data losses, we use the `SmoothL1Loss()` loss function from *PyTorch* [50], which is less sensitive to outliers than the mean squared error loss. The parameter β in the `SmoothL1Loss()` function, which controls the transition between the mean absolute and mean squared error, was empirically set for each data type individually.

$\mathcal{L}_{\text{TPXY}}$ penalizes the average deviation of the two logarithmic activity coefficients predicted with HANNA from the respective experimental values derived from the TPXY data for the binary systems from the training set:

$$\mathcal{L}_{\text{TPXY}} = \sum_k^{N_{\text{TPXY}}} \text{SmoothL1Loss}([\ln \gamma_{1,\text{pred}}, \ln \gamma_{2,\text{pred}}], [\ln \gamma_{1,\text{exp}}, \ln \gamma_{2,\text{exp}}]) \quad (7) \\ \text{with } \beta = 1.0$$

where N_{TPXY} is the number of TPXY data points in the training batch.

Similarly, \mathcal{L}_{ACI} takes into account errors in the prediction of the activity coefficients at infinite dilution $\ln \gamma_i^\infty$ for the binary systems from the training set:

$$\mathcal{L}_{\text{ACI}} = \frac{1}{2} \sum_k^{N_{\text{ACI}}} \text{SmoothL1Loss}(\ln \gamma_{i,\text{pred}}^\infty, \ln \gamma_{i,\text{exp}}^\infty) \quad \text{with } \beta = 2.0 \quad (8)$$

where N_{ACI} is the number of ACI data points in the batch. The factor $\frac{1}{2}$ takes into account that in \mathcal{L}_{ACI} , only the activity coefficient at infinite dilution contributes to the loss calculation, whereas in $\mathcal{L}_{\text{TPXY}}$, the errors of both activity coefficients of the binary mixture are averaged before contributing to the loss.

\mathcal{L}_{TPX} accounts for the difference of the predicted logarithmic total pressures to the experimental ones on the N_{TPX} TPX data points:

$$\mathcal{L}_{\text{TPX}} = \sum_k^{N_{\text{TPX}}} \text{SmoothL1Loss}(\ln(p_{\text{pred}}/\text{bar}), \ln(p_{\text{exp}}/\text{bar})) \quad \text{with } \beta = 1.0 \quad (9)$$

The predicted logarithmic total pressures are calculated from the predicted activity coefficients and the pure component vapor pressures:

$$\ln(p_{\text{pred}}/\text{bar}) = \ln\left(\frac{p_1^{\text{s}}x_1\gamma_{1,\text{pred}} + p_2^{\text{s}}x_2\gamma_{2,\text{pred}}}{\text{bar}}\right) \quad (10)$$

\mathcal{L}_{LLE} denotes the loss between the LLE phase compositions in mole fractions predicted by HANNA and the experimental values in the batch obtained through

$$\mathcal{L}_{\text{LLE}} = \sum_k^{N_{\text{LLE}}} m_k \cdot \text{SmoothL1Loss}([x'_{1,\text{pred}}, x''_{1,\text{pred}}], [x'_{1,\text{exp}}, x''_{1,\text{exp}}]) \quad (11)$$

with $\beta = 0.35$

where N_{LLE} is the number of LLE data points in the batch and $m_k \in \{0, 1\}$ is a binary mask that indicates if the respective data point is considered or not (cf. below for details). To obtain the predicted phase compositions $x'_{1,\text{pred}}, x''_{1,\text{pred}}$ for a data point during training, the pre-trained surrogate solver (cf. Section 4.3) is provided with the discretized molar Gibbs energy of mixing curve for the respective system and temperature. For the LLE data points with only one available phase composition, the loss term in Eq. 11 is calculated only on this phase composition. Since the surrogate solver is only trained on positive samples (i.e., binary LLE systems at state points with a miscibility gap) and cannot identify systems without miscibility gap, it will also falsely predict a phase split for a Δg_{mix} that does not fulfill the necessary condition for a phase split, which states

$$\left(\frac{\partial^2 \Delta g_{\text{mix}}}{\partial x_1^2}\right)_{T,p} < 0 \quad (12)$$

i.e., the second derivative of Δg_{mix} is negative somewhere in the composition space. This is unphysical and could potentially negatively impact the training process. Therefore, during the training, we account for the LLE loss of binary systems only if the necessary condition in Eq. (12) is true for at least one discretized composition; this is reflected in Eq. (11) through the binary mask m_k , where $m_k = 1$ for data points that exhibit an LLE and $m_k = 0$ for those that do not. The required second derivatives of Δg_{mix} were calculated by automatic differentiation. \mathcal{L}_{HE} describes the loss on the

N_{HE} excess enthalpy data points:

$$\mathcal{L}_{\text{HE}} = \sum_k^{N_{\text{HE}}} \text{SmoothL1Loss}(h_{\text{pred}}^{\text{E}}, h_{\text{exp}}^{\text{E}}) \quad \text{with } \beta = 2.0 \quad (13)$$

The predicted excess enthalpy is calculated using [40]

$$h_{\text{pred}}^{\text{E}} = -RT^2 \left(\frac{\partial}{\partial T} \frac{g_{\text{pred}}^{\text{E}}}{RT} \right)_x = -\frac{RT^2}{s_T} \left(\frac{\partial}{\partial T^*} \frac{g_{\text{pred}}^{\text{E}}}{RT} \right)_x \quad (14)$$

The factor $1/s_T$ in Eq. (14) follows from the chain rule because HANNA uses the scaled temperature $T^* = (T - \mu_T)/s_T$ as input.

Gibbs Loss

The \mathcal{L}_{LLE} described above alone does not penalize false negative LLE predictions. If HANNA fails to predict a liquid-liquid phase split, the necessary condition in Eq. (12) is not fulfilled and the binary mask is $m_k = 0$, cf. Eq. 11. To provide a learning incentive towards a correct detection of these phase splits, the additional loss term $\mathcal{L}_{\text{Gibbs}}$ was introduced:

$$\mathcal{L}_{\text{Gibbs}} = \sum_k^{N_{\text{LLE}}} \max \left(0, \min_d S_k(T_k, x_{1,d}) \right) \quad (15)$$

Here,

$$S_k(T_k, x_{1,d}) = \frac{1}{RT_k} \left(\frac{\partial^2 \Delta g_{\text{mix}}(T_k, x_{1,d})}{\partial x_1^2} \right)_T \quad (16)$$

is the second derivative of the molar Gibbs energy of mixing for data point k from the LLE training set evaluated at the composition d on the discretized grid of Δg_{mix} . Eq. 15 identifies the minimum of the second derivative of Δg_{mix} within the discretized composition space for each LLE training data point. If this minimum is negative, a miscibility gap is predicted by the model (cf. Eq. (12)) and the Gibbs loss is zero.² On the other hand, if the minimum is positive, the miscibility gap is not identified by HANNA, and, consequently, the model is penalized by adding the respective value of S_k to the total loss.

Lipschitz Regularization

Besides the data losses and the Gibbs loss, $\mathcal{L}_{\text{Lips}}$ is included in the total loss function as a Lipschitz regularization term, controlling the Lipschitz constant of HANNA. Generally, the Lipschitz constant ($c \geq 0$) in the 2-norm is defined as

$$\|f(x_1) - f(x_0)\|_2 \leq c \|x_1 - x_0\|_2 \quad (17)$$

²Note that in this case ($m_k = 1$) the deviation to experimental data is accounted for by \mathcal{L}_{LLE} .

and provides an upper bound for the change of a function from $f(x_0)$ to $f(x_1)$ by changing the function input from x_0 to x_1 ; it is, therefore, a proxy for the smoothness of a function. For fully connected neural networks with L layers, a loose upper bound

$$c = \prod_{l=1}^L c_l = \prod_{l=1}^L \|\mathbf{W}_l\|_2 = \prod_{l=1}^L \sigma_{\max}(\mathbf{W}_l) \quad (18)$$

is obtained by the product of the spectral norms $\|\mathbf{W}_l\|_2$ of the weight matrices of each layer l , if the Lipschitz constants of the activation functions are neglected [60]. For HANNA, the influence of the summation of the two mixture embeddings (cf. step 10 in Algorithm 1) on the total Lipschitz constant is also neglected, since it does not contain any learnable parameters. The spectral 2-norm $\|\mathbf{W}_l\|_2$, in turn, equals the maximum singular value $\sigma_{\max}(\mathbf{W}_l)$ of the weight matrix \mathbf{W}_l [61].

Following the approach from Ref. [60], all networks of HANNA are realized as modified linear layers with learnable Lipschitz constants c_l^* . In these layers, the raw weight matrices \mathbf{W}_{raw} are first normalized using the maximum singular value $\sigma_{\max}(\mathbf{W}_{l,\text{raw}})$ (such that their Lipschitz constant equals one) and then scaled using the learnable Lipschitz constants :

$$\mathbf{W}_{l,\text{scaled}} = \frac{\mathbf{W}_{l,\text{raw}}}{\sigma_{\max}(\mathbf{W}_{l,\text{raw}})} \cdot \text{softplus}(c_l^*) \quad (19)$$

These scaled weight matrices are then used in the forward function of the modified layers as a drop-in replacement of the raw weight matrices. For computational efficiency, we approximate $\sigma_{\max}(\mathbf{W}_{l,\text{raw}})$ with a power iteration method using two iterations [61]. The Lipschitz regularization term used in the total loss function, cf. Eq. (6), is calculated via [60]

$$\mathcal{L}_{\text{Lips}} = \prod_{l=1}^L \text{softplus}(c_l^*) \quad (20)$$

by multiplying the total Lipschitz constants of the networks (given by the product of the layer-wise learned constants of all L layers in the model and ignoring other factors, cf. above). The softplus transformation of c_l^* avoids infeasible negative Lipschitz constants [60]. The hyperparameter w_{Lips} , cf. Eq. (6), can be used to control the learnable Lipschitz constants of the network, i.e., higher values of w_{Lips} lead to lower Lipschitz constants and vice versa. For the model variants in the grid search with $w_{\text{Lips}} = 0$, we employed a L2-regularization instead to prevent exploding parameters.

Training Details

The HANNA models for this work were trained for 200 epochs using a batch size of 512, the AdamW optimizer and the OneCycleLR scheduler (`max_lr=0.01`) from PyTorch. The best epoch was selected based on the weighted sum of the data losses

($\mathcal{L}_{\text{TPXY}}$, \mathcal{L}_{TPX} , \mathcal{L}_{ACI} , \mathcal{L}_{LLE} and \mathcal{L}_{HE}) on the respective validation set, whereby only models that were trained for at least 50 epochs were considered.

After determining the optimal hyperparameters through a grid search (cf. section "Grid search" in the Supplementary Information), we trained an ensemble of ten models (starting from different weight initializations) for each data fold (cf. Section 4.2). Additionally, we trained such an ensemble for the full data split; this model is also published as final model along this work. Training was carried out on NVIDIA A30 GPUs; a typical training run of a single HANNA model (200 epochs) required approximately 20 hours.

4.5 Evaluation of HANNA

For the systematic evaluation of HANNA and the benchmark models, absolute deviations ϵ between the predicted and the experimental values for each data point in the considered test set were calculated.

For each TPXY data point, a mean absolute deviation of the logarithmic activity coefficients of all components i in the test mixture at the respective temperature T and composition \mathbf{x} was calculated:

$$\epsilon_{\text{TPXY}} = \frac{1}{N} \sum_{i=1}^N \left| \ln \gamma_i^{\text{pred}} - \ln \gamma_i^{\text{exp}} \right| \quad (21)$$

Here, N is the number of components in the mixture ($N = 2$ for binary, $N = 3$ for ternary, $N = 4$ for quaternary mixtures).

To evaluate the model performance on the TPX data points, the absolute deviations in the logarithmic total pressures were calculated:

$$\epsilon_{\text{TPX}} = \left| \ln (p^{\text{pred}}/\text{bar}) - \ln (p^{\text{exp}}/\text{bar}) \right| \quad (22)$$

For each ACI data point, i.e., activity coefficients at infinite dilution in pure or in mixed solvents, only the logarithmic activity coefficient of the infinitely diluted solute i in the solvent(s) was considered for error calculation:

$$\epsilon_{\text{ACI}} = \left| \ln \gamma_i^{\text{pred},\infty} - \ln \gamma_i^{\text{exp},\infty} \right| \quad (23)$$

The LLE predictions were evaluated through the mean absolute deviation of the phase compositions in mole fractions x'_i and x''_i (and x'''_i for three-phase equilibria) of all components i in the mixture:

$$\epsilon_{\text{LLE}} = \frac{1}{2N} \sum_{i=1}^N \left| x'_{i,\text{pred}} - x'_{i,\text{exp}} \right| + \left| x''_{i,\text{pred}} - x''_{i,\text{exp}} \right| + \left| x'''_{i,\text{pred}} - x'''_{i,\text{exp}} \right| \quad (24)$$

For the HE data, the absolute deviation of the excess enthalpies in kJ mol^{-1} was used as evaluation metric:

$$\epsilon_{\text{HE}} = \left| \frac{h_{\text{pred}}^{\text{E}} - h_{\text{exp}}^{\text{E}}}{\text{kJ mol}^{-1}} \right| \quad (25)$$

From the data point-wise error scores described above, system-wise mean absolute error MAE_{sys} scores were calculated by averaging over all data points (at all temperatures and compositions) for each binary, ternary, or quaternary system. The system-wise error scores are favorable as they are independent of the number of available data points for a particular system and do not over-emphasize systems with many data points, such as (ethanol + water). Therefore, they are more suitable to evaluate the performance of the models to generalize over unseen systems and components.

The HANNA predictions shown in the evaluation of this work were obtained using ensembles of ten individual models. For the binary data, we used the ten independently trained ensembles and evaluated them on their respective test set. For the multi-component data, the final model, i.e., the ensemble trained on the full data split, was used.

Data Availability

The thermodynamic data used in this study were obtained from the Dortmund Data Bank (DDBST GmbH, Oldenburg, Germany) under a proprietary license and are therefore not publicly available and cannot be shared by the authors. Access to DDB can be obtained directly from DDBST GmbH (<https://www.ddbst.com>) subject to a license agreement and associated fees. Source Data are provided with this paper.

Code Availability

The HANNA model class and trained parameters of the final model are available at <https://github.com/marco-hoffmann/HANNA>. Example code to generate predictions for excess Gibbs energies, activity coefficients and excess enthalpies in binary and multi-component mixtures is provided in the repository.

References

- [1] Renon, H. & Prausnitz, J. M. Local compositions in thermodynamic excess functions for liquid mixtures. *AIChE Journal* **14**, 135–144 (1968).
- [2] Abrams, D. S. & Prausnitz, J. M. Statistical thermodynamics of liquid mixtures: a new expression for the excess gibbs energy of partly or completely miscible systems. *AIChE Journal* **21**, 116–128 (1975).
- [3] Rarey, J. Extended flexibility for g^{E} models and simultaneous description of vapor-liquid equilibrium and liquid-liquid equilibrium using a nonlinear transformation of the concentration dependence. *Industrial & Engineering Chemistry Research* **44**, 7600–7608 (2005).

- [4] Marcilla, A., Olaya, M. & Reyes-Labarta, J. Simultaneous vllc data correlation for ternary systems: modification of the nrtl equation for improved calculations. *Fluid Phase Equilibria* **426**, 47–55 (2016).
- [5] Fredenslund, A., Jones, R. L. & Prausnitz, J. M. Group-contribution estimation of activity coefficients in nonideal liquid mixtures. *AIChE Journal* **21**, 1086–1099 (1975).
- [6] Wittig, R., Lohmann, J. & Gmehling, J. Vapor-liquid equilibria by unifac group contribution. 6. revision and extension. *Industrial & Engineering Chemistry Research* **42**, 183–188 (2002).
- [7] Weidlich, U. & Gmehling, J. A modified unifac model. 1. prediction of vle, h^e , and γ^∞ . *Industrial & Engineering Chemistry Research* **26**, 1372–1381 (1987).
- [8] Constantinescu, D. & Gmehling, J. Further development of modified unifac (dortmund): revision and extension 6. *Journal of Chemical & Engineering Data* **61**, 2738–2748 (2016).
- [9] Magnussen, T., Rasmussen, P. & Fredenslund, A. Unifac parameter table for prediction of liquid-liquid equilibria. *Industrial & Engineering Chemistry Process Design and Development* **20**, 331–339 (1981).
- [10] Lei, Z., Zhang, J., Li, Q. & Chen, B. Unifac model for ionic liquids. *Industrial & Engineering Chemistry Research* **48**, 2697–2704 (2009).
- [11] Zhu, R. *et al.* Unifac model for ionic liquids: 3. revision and extension. *Industrial & Engineering Chemistry Research* **63**, 1670–1679 (2024).
- [12] Schmitz, N., Friebel, A., von Harbou, E., Burger, J. & Hasse, H. Liquid-liquid equilibrium in binary and ternary mixtures containing formaldehyde, water, methanol, methylal, and poly(oxyethylene) dimethyl ethers. *Fluid Phase Equilibria* **425**, 127–135 (2016).
- [13] Schmitz, N., Breitzkreuz, C. F., Ströfer, E., Burger, J. & Hasse, H. Vapor-liquid equilibrium and distillation of mixtures containing formaldehyde and poly(oxyethylene) dimethyl ethers. *Chemical Engineering and Processing - Process Intensification* **131**, 116–124 (2018).
- [14] Klamt, A. & Schüürmann, G. Cosmo: a new approach to dielectric screening in solvents with explicit expressions for the screening energy and its gradient. *J. Chem. Soc., Perkin Trans. 2* 799–805 (1993).
- [15] Klamt, A. Conductor-like screening model for real solvents: a new approach to the quantitative calculation of solvation phenomena. *The Journal of Physical Chemistry* **99**, 2224–2235 (1995).

- [16] Lin, S.-T. & Sandler, S. I. A priori phase equilibrium prediction from a segment contribution solvation model. *Industrial & Engineering Chemistry Research* **41**, 899–913 (2001).
- [17] Grensemann, H. & Gmehling, J. Performance of a conductor-like screening model for real solvents model in comparison to classical group contribution methods. *Industrial & Engineering Chemistry Research* **44**, 1610–1624 (2005).
- [18] Wang, S., Stubbs, J. M., Siepmann, J. I. & Sandler, S. I. Effects of conformational distributions on sigma profiles in cosmo theories. *The Journal of Physical Chemistry A* **109**, 11285–11294 (2005).
- [19] Mu, T., Rarey, J. & Gmehling, J. Performance of cosmo-rs with sigma profiles from different model chemistries. *Industrial & Engineering Chemistry Research* **46**, 6612–6629 (2007).
- [20] Franke, R. & Hannebauer, B. On the influence of basis sets and quantum chemical methods on the prediction accuracy of cosmo-rs. *Physical Chemistry Chemical Physics* **13**, 21344 (2011).
- [21] Fingerhut, R. *et al.* Comprehensive assessment of cosmo-sac models for predictions of fluid-phase equilibria. *Industrial & Engineering Chemistry Research* **56**, 9868–9884 (2017).
- [22] Xue, Z., Mu, T. & Gmehling, J. Comparison of the a priori cosmo-rs models and group contribution methods: original unifac, modified unifac(do), and modified unifac(do) consortium. *Industrial & Engineering Chemistry Research* **51**, 11809–11817 (2012).
- [23] Jirasek, F. *et al.* Making thermodynamic models of mixtures predictive by machine learning: matrix completion of pair interactions. *Chemical Science* **13**, 4854–4862 (2022).
- [24] Winter, B., Winter, C., Esper, T., Schilling, J. & Bardow, A. Spt-nrtl: a physics-guided machine learning model to predict thermodynamically consistent activity coefficients. *Fluid Phase Equilibria* **568**, 113731 (2023).
- [25] Hayer, N., Wendel, T., Mandt, S., Hasse, H. & Jirasek, F. Advancing thermodynamic group-contribution methods by machine learning: Unifac 2.0. *Chemical Engineering Journal* **504**, 158667 (2025).
- [26] Hayer, N., Hasse, H. & Jirasek, F. Modified unifac 2.0-a group-contribution method completed with machine learning. *Industrial & Engineering Chemistry Research* **64**, 10304–10313 (2025).
- [27] Sanchez Medina, E. I., Linke, S., Stoll, M. & Sundmacher, K. Graph neural networks for the prediction of infinite dilution activity coefficients. *Digital Discovery*

- 1, 216–225 (2022).
- [28] Sanchez Medina, E. I., Linke, S., Stoll, M. & Sundmacher, K. Gibbs–helmholtz graph neural network: capturing the temperature dependency of activity coefficients at infinite dilution. *Digital Discovery* **2**, 781–798 (2023).
- [29] Qin, S. *et al.* Capturing molecular interactions in graph neural networks: a case study in multi-component phase equilibrium. *Digital Discovery* **2**, 138–151 (2023).
- [30] Rittig, J. G., Felton, K. C., Lapkin, A. A. & Mitsos, A. Gibbs–duhem-informed neural networks for binary activity coefficient prediction. *Digital Discovery* **2**, 1752–1767 (2023).
- [31] Rittig, J. G. & Mitsos, A. Thermodynamics-consistent graph neural networks. *Chemical Science* **15**, 18504–18512 (2024).
- [32] Specht, T. *et al.* Hanna: hard-constraint neural network for consistent activity coefficient prediction. *Chemical Science* **15**, 19777–19786 (2024).
- [33] Weininger, D. Smiles, a chemical language and information system. 1. introduction to methodology and encoding rules. *Journal of Chemical Information and Computer Sciences* **28**, 31–36 (1988).
- [34] Ahmad, W., Simon, E., Chithrananda, S., Grand, G. & Ramsundar, B. Chemberta-2: towards chemical foundation models (2022). Preprint at <https://arxiv.org/abs/2209.01712>.
- [35] Muggianu, Y.-M., Gambino, M. & Bros, J.-P. Enthalpies de formation des alliages liquides bismuth–étain–gallium à 723 k. choix d’une représentation analytique des grandeurs d’excès intégrales et partielles de mélange. *Journal de Chimie Physique* **72**, 83–88 (1975).
- [36] Ryll, O., Blagov, S. & Hasse, H. Convex envelope method for the determination of fluid phase diagrams. *Fluid Phase Equilibria* **324**, 108–116 (2012).
- [37] Göttl, Q., Pirnay, J., Grimm, D. G. & Burger, J. Convex envelope method for determining liquid multi-phase equilibria in systems with arbitrary number of components. *Computers & Chemical Engineering* **177**, 108321 (2023).
- [38] Göttl, Q., Rosen, N. & Burger, J. Convex envelope method for t, p flash calculations for mixtures with an arbitrary number of components and arbitrary aggregate states. *Computers & Chemical Engineering* 109326 (2025).
- [39] Dortmund data bank. <https://www.ddbst.com> (2025).
- [40] Gmehling, J., Kleiber, M., Kolbe, B. & Rarey, J. *Chemical thermodynamics for process simulation* 2 edn (John Wiley & Sons, 2019).

- [41] Klamt, A., Krooshof, G. J. P. & Taylor, R. Cosmospace: alternative to conventional activity-coefficient models. *AIChE Journal* **48**, 2332–2349 (2002).
- [42] Ju, T., Ding, X., Chen, W., Yan, X. & Dong, Y. A new perspective on geometric thermodynamic models. *Journal of Phase Equilibria and Diffusion* **40**, 715–724 (2019).
- [43] Ju, T., Huang, Z., Ding, X., Yan, X. & Liao, C. A unified extrapolation thermodynamic model for multicomponent solutions based on binary data. *Thermochimica Acta* **740**, 179824 (2024).
- [44] Huggingface chemberta-2 model. <https://huggingface.co/DeepChem/ChemBERTa-77M-MTR>. Last accessed: 08.07.2025.
- [45] Antolović, I., Stephan, S. & Vrabec, J. High-throughput application and evaluation of the cosmo-sac model for predictions of liquid–liquid equilibria. *Digital Discovery* **4**, 3191–3207 (2025).
- [46] Gmehling, J., Wittig, R., Lohmann, J. & Joh, R. A modified unifac (dortmund) model. 4. revision and extension. *Industrial & Engineering Chemistry Research* **41**, 1678–1688 (2002).
- [47] Yüksel, A., Ulusoy, E., Ünlü, A. & Doğan, T. Selfformer: molecular representation learning via selfies language models. *Machine Learning: Science and Technology* **4**, 025035 (2023).
- [48] Krenn, M., Häse, F., Nigam, A., Friederich, P. & Aspuru-Guzik, A. Self-referencing embedded strings (selfies): a 100% robust molecular string representation. *Machine Learning: Science and Technology* **1**, 045024 (2020).
- [49] Duvenaud, D. *et al.* Convolutional networks on graphs for learning molecular fingerprints (2015). Preprint at <https://arxiv.org/abs/1509.09292>.
- [50] Paszke, A. *et al.* Pytorch: an imperative style, high-performance deep learning library (2019). Preprint at <https://arxiv.org/abs/1912.01703>.
- [51] RDKit: open-source cheminformatics. <http://www.rdkit.org>. Version: 2023.03.1.
- [52] Pelton, A. D. A general “geometric” thermodynamic model for multicomponent solutions. *Calphad* **25**, 319–328 (2001).
- [53] Luo, Q., Zhai, C., Sun, D., Chen, W. & Li, Q. Interpolation and extrapolation with the calphad method. *Journal of Materials Science & Technology* **35**, 2115–2120 (2019).
- [54] Chartrand, P. & Pelton, A. D. On the choice of “geometric” thermodynamic models. *Journal of Phase Equilibria* **21**, 141–147 (2000).

- [55] Cheng, W. & Ganguly, J. Some aspects of multicomponent excess free energy models with subregular binaries. *Geochimica et Cosmochimica Acta* **58**, 3763–3767 (1994).
- [56] Howald, R. A. & Roy, B. N. Muggianu and toop-muggianu interpolations comment on a comment by I. Kaufman (Calphad, 225 (1981)) on Brynestad’s paper (Calphad, 103 (1981)). *Calphad* **6**, 57–63 (1982).
- [57] Zaheer, M. *et al.* Deep sets (2017). Preprint at <https://arxiv.org/abs/1703.06114>.
- [58] Deiters, U. K. & Kraska, T. *High-pressure fluid phase equilibria* (Elsevier Science & Technology Books, 2012).
- [59] Pedregosa, F. *et al.* Scikit-learn: machine learning in python. *Journal of Machine Learning Research* **12**, 2825–2830 (2011).
- [60] Liu, H.-T. D., Williams, F., Jacobson, A., Fidler, S. & Litany, O. Learning smooth neural functions via Lipschitz regularization (2022). Preprint at <https://arxiv.org/abs/2202.08345>.
- [61] Miyato, T., Kataoka, T., Koyama, M. & Yoshida, Y. Spectral normalization for generative adversarial networks (2018). Preprint at <https://arxiv.org/abs/1802.05957>.

Acknowledgments

We gratefully acknowledge financial support by the Carl Zeiss Foundation in the frame of the project ‘Process Engineering 4.0’ and by DFG in the frame of the Priority Program SPP2363 ‘Molecular Machine Learning’ (grant number 497201843). Furthermore, FJ gratefully acknowledges financial support by DFG in the frame of the Emmy-Noether program (grant number 528649696). Model training and evaluation was carried out on the high performance computer Elwetrisch at RPTU under the grant RPTU-MLVT. We thank Jan Rittig for providing us with parameter sets of GDI-GNN and GE-GNN for evaluation.

Author Contributions

M.H.: Conceptualization; Methodology; Software; Validation; Formal analysis; Investigation; Data curation; Writing – original draft; Visualization. T.S.: Conceptualization; Methodology; Software; Validation; Formal analysis; Investigation; Data curation; Writing – original draft. Q.G.: Methodology; Software. Writing – review & editing. J.B.: Methodology; Writing – review & editing. S.M.: Conceptualization; Methodology; Writing – review & editing. H.H.: Conceptualization; Writing – review & editing; Supervision; Project administration; Funding acquisition. F.J.: Conceptualization; Methodology; Writing – review & editing; Supervision; Project administration; Funding acquisition.

Declaration of Competing Interests

The authors declare no competing interests.